

---

# Blind Deconvolution of turbulence flows using Neural Networks

---

Anonymous Author(s)

Affiliation

Address

email

## Abstract

1

## 2 1 Problem background

### 3 1.1 Convolution and Deconvolution

4 In applied mathematics and computer science (and, in particular, functional analysis) convolution is a  
5 mathematical operation on two functions ( $f$  and  $g$ ) that produces a third function, which is typically  
6 viewed as a modified version of one of the original functions. This modified function gives the  
7 integral of the point-wise multiplication of the two functions as a function of the amount that one of  
8 the original functions has been translated.

9 The convolution of  $f$  and  $g$  is written  $f * g$ , using an  $[*]$  or star. It is defined as the integral of the  
10 product of the two functions after one is reversed and shifted. As such, it is a particular kind of  
11 [[integral transform]]:

$$\begin{aligned} 12 \quad (f * g)(t) &\stackrel{\text{def}}{=} \int_{-\infty}^{\infty} f(\tau)g(t - \tau) d\tau \\ 13 &= \int_{-\infty}^{\infty} f(t - \tau)g(\tau) d\tau. \end{aligned}$$

14 Deconvolution, on the other hand is an algorithm-based process used to reverse the effects of  
15 convolution on recorded data. The concept of deconvolution is extensively used in the techniques of  
16 signal processing and image processing.

### 17 1.2 Turbulence modeling and the Closure Problem

18 In fluid dynamics, turbulence or turbulent flow is any pattern of fluid motion characterized by chaotic  
19 changes in pressure and flow velocity. It is in contrast to a laminar flow regime, which occurs when a  
20 / the fluid flows in parallel layers, with no disruption between those layers.

21 In Turbulence modeling, one constructs and uses a model to predict the effects of turbulence. A  
22 turbulent fluid flow has features on many different length scales, which all interact with each other. A  
23 common or naive approach is to average the governing equations of the flow, in order to focus on  
24 large-scale and non-fluctuating features of the flow.

25 The velocity and pressure of a fluid flow is governed by the Navier–Stokes equations. In a turbulent  
26 flow, each of these quantities may be decomposed into a mean part and a fluctuating part. On  
27 averaging the equations, we get the Reynolds-averaged Navier–Stokes (RANS) equations, which  
28 govern the mean flow. The non-linearity of the Navier–Stokes equations however means that the  
29 velocity fluctuations still appear in the RANS equations, in the nonlinear term  $\overline{\rho v'_i v'_j}$  from the  
30 convective acceleration. This term is known as the Reynolds stress,  $R_{ij}$ . [2] Its effect on the mean  
31 flow is like that of a stress term, such as from pressure or viscosity.

32 To obtain equations containing only the mean velocity and pressure, we need to close the RANS  
33 equations by modelling the Reynolds stress term  $R_{ij}$  as a function of the mean flow, removing any  
34 reference to the fluctuating part of the velocity. This is the closure problem.

## 35 2 Our Objectives

36 The major motivation for this project is due to the recent advances in the image processing community  
37 which employ general machine learning techniques used for reconstruction of noisy or blurred images.  
38 In particular, our objective is to implement Artificial Neural Network (ANN)-based machine learning  
39 strategies to recover subfilter-scale features in turbulence closure modeling.

40 We aim to develop a single-layer feed forward ANN to identify a non-linear relationship between  
41 the low-pass spatially filtered and coarse-grained (but unfiltered) field variables for settings in two-  
42 dimensional (2D) and three-dimensional (3D) homogenous isotropic turbulence as well as a stratified  
43 turbulence case exhibiting moderate compressibility in the limit of infinite Reynold's numbers.

44 The approach outlined in our study is analogous to the approximate deconvolution methodology  
45 (Stolz and Adams 1999) to recover subfilter contributions of low-pass spatially filtered flow fields,  
46 and the only difference is the lack of assumption of any filtering kernel (Gaussian or otherwise) -  
47 which is why we call the deconvolution 'blind'.

## 48 3 Approach

49 The first step was to import and preprocessed the data - we extracted the dataset (described below)  
50 from the JHTDB website, and pre-processed it by using the shifting strategy, filtering it and finally  
51 generating the training and test sets for our algorithms.

### 52 3.1 The Dataset

53 The datasets we used were taken from the John Hopkins Turbulence Databases  
54 (<http://turbulence.pha.jhu.edu/>) -

55 **Forced isotropic turbulence** which was generated from direct numerical simulation (DNS) using  
56  $1,024^3$  nodes. Here the Navier-Stokes equation was solved using pseudo-spectral method, and the  
57 energy was injected by keeping constant the total energy in shells such that  $|k|$  is less or equal to  
58 2. After the simulation reached a statistical stationary state, 5,028 frames of data with 3 velocity  
59 components and pressure were stored in the database. The Taylor-scale Reynolds number fluctuates  
60 around  $R = 433$ . In one dataset ("coarse") there are 5028 timesteps available, for time  $t$  between 0 and  
61 10.056 (the frames are stored at every 10 time-steps of the DNS) and the intermediate times can be  
62 queried using temporal-interpolation. In the other dataset ("fine"), single time-step of the DNS is  
63 stored, for testing purposes. Times available are for  $t$  between 0.0002 and 0.0198). This data was  
64 used for the 3D case.

65 **Forced Isotropic Turbulence Dataset on  $4096^3$  Grid** which was generated from direct numerical  
66 simulation (DNS) using  $4096^3$  nodes. The Navier-Stokes equation was solved using pseudo-spectral  
67 method, and the time integration uses second-order Runge-Kutta method. While the simulation is  
68 de-aliased using phase-shifting and truncation, energy is injected by keeping the energy density in the  
69 lowest wavenumber modes prescribed following the approach of Donzis Yeung. After the simulation  
70 reached a statistical stationary state, a frame of data, which includes the 3 components of the velocity  
71 vector and the pressure, were generated and written in files that could be accessed directly by the  
72 database (FileDB system).

### 73 3.2 Data Preprocessing

74 The 3D numerical experiments were generated using  $512^3$  degrees of freedom while the 2D case was  
75 generated using  $2048^2$  grid points. A coarse-grained large eddy simulation was mimicked through  
76 the subsequent sampling of these high-quality datasets. The coarse-graining procedure was then  
77 applied with a sub-sampled field of  $64^3$  and  $256^2$  degrees of freedom in the 3D and 2D test cases,  
78 respectively. In other words, our coarse-graining procedure involves the selection of every eighth  
79 point in the high-fidelity uniform grid data.

80 We devised several shifted data sets (each possessing  $64^3$  degrees of freedom in 3D and  $256^2$  degrees  
81 of freedom in 2D) which continue to represent the physics of the fine-grained dataset. The missing  
82 data points at boundaries were reconstructed through the use of the periodic boundary conditions for  
83 the given test cases. A simplified shifting schematic was employed (shown in figure 1 below),

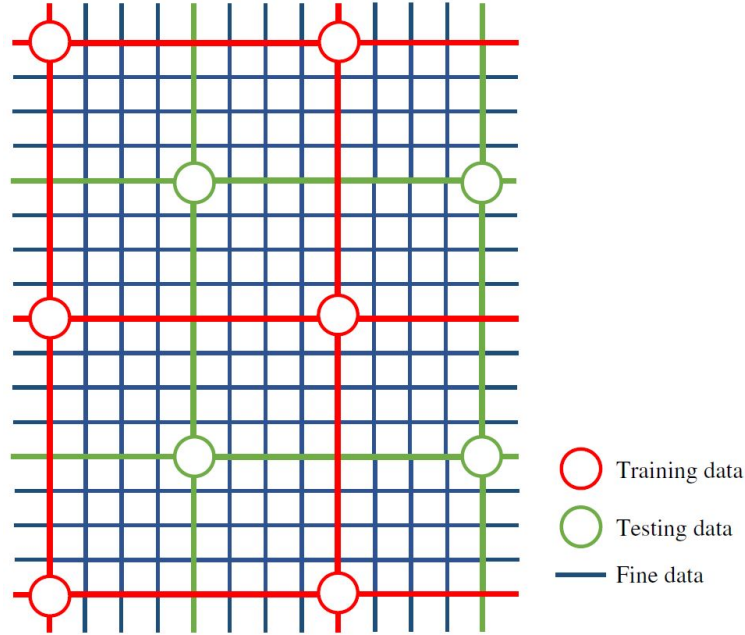


Figure 1: Schematic of spatial shifting strategy for a simplified two-dimensional grid showing two different data-sets

84 where a simple technique of generating two coarse data sets from fine data is demonstrated. In short,  
85 the coarse-graining and shifting procedures allow us to devise up to 63 and 511 completely different  
86 data sets in two and three dimensions, respectively. For cross-validation we randomly chose any four  
87 of these multiple data sets for the generation of three sets of testing data and one set of training data.

88 After our four different randomly generated data sets are identified, we added perturbations corre-  
89 sponding to the type of behaviour demanded of the proposed artificial neural network. To test the  
90 deconvolution ability of our network, our training data (i.e., one of the four data sets) was filtered  
91 with an appropriate Gaussian smoothing (for our inputs to the network) and unfiltered training data  
92 were utilized as outputs to the network. Three testing data sets are generated in a similar manner,  
93 with one of these data sets being filtered with the same filter radius and the others being filtered with  
94 a 10% larger and 10% smaller filter radius, respectively (Figure 2).

95 The trained ANN was then utilized to recover deconvolved approximations to the true field for these  
96 three test data sets. This ensured that the trends of the trained network were not due to overfitting or  
97 ‘data-memory’ but through an implicit learning of the inverse filtering. A similar procedure was also  
98 utilized to cross-validate the regularization ability of the closure wherein the randomly chosen data  
99 sets were perturbed through Gaussian noise. A table describing the filter radii and magnitudes of  
100 noise for our training and testing data sets is shown in Figure 3 below.

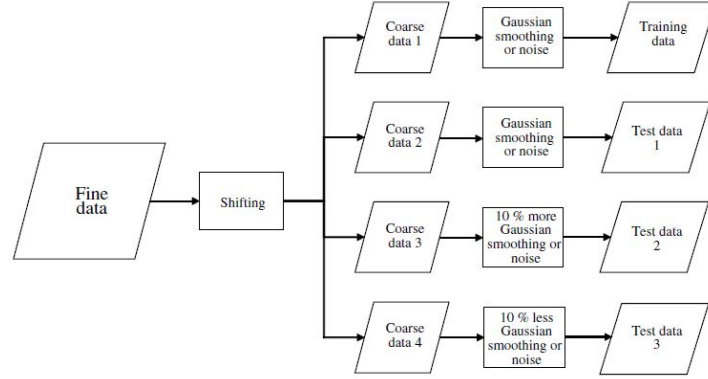


Figure 2: A flow chart explaining the generation of cross-validation data sets using the shifting operation and different perturbations.

Deconvolution		Regularization	
Data set	Filter radius ( $\sigma$ )	Data set	Noise ( $\mu$ )
Training data	1.0	Training data	0.2
Test data 1	1.0	Test data 1	0.2
Test data 2	1.1	Test data 2	0.22
Test data 3	0.9	Test data 3	0.18

Figure 3: Cross-validation data sets for the proposed data-driven blind deconvolution closure

#### 101 **4 Extreme learning machine**

#### 102 **5 Single layer feed-forward NN with keras**

#### 103 **6 Two layer feed-forward NN with keras**

#### 104 **7 Results**

#### 105 **8 Conclusion**

#### 106 **9 References**

107 [1] <https://en.wikipedia.org/wiki/Convolution>

108 [2] <https://en.wikipedia.org/wiki/Deconvolution>

109 [3] <https://en.wikipedia.org/wiki/Turbulence>

110 [4] A neural network approach for the blind deconvolution of turbulent flows,R. Maulik and  
 111 O. San, Journal of Fluid Mechanics, Get access Volume 831,25 November 2017, pp. 151-181,  
 112 <https://doi.org/10.1017/jfm.2017.637>